

# PLASMA CLEANING OF HYDROCARBON AND CARBON CONTAMINATED SURFACES OF ACCELERATOR COMPONENTS

M. C. Giordano\*, P. Costa Pinto, B. Henrist, M. Himmerlich, M. Taborelli, N. Thaus,  
European Organization for Nuclear Research, CERN, Geneva, Switzerland  
V. Carlino, M. Fahey, J. Monteiro, L. Tran, ibss Group Inc., Burlingame, CA 94010, USA

## Abstract

To achieve the vacuum quality required for the operation of particle accelerators, the surface of the vacuum vessels must be clean from hydrocarbons. This is usually achieved by wet chemistry processes, e.g. degreasing chemical baths that, in case of radioactive vessels, must be disposed accordingly. An alternative way exploits the oxygen plasma produced by a downstream RF plasma source. This technique offers the possibility of operating in-situ, which is an advantageous option to avoid the handling of voluminous and/or fragile components and a more sustainable alternative to large volume disposable baths. In this work, we test a commercial plasma source in dedicated vacuum systems equipped with quartz crystal microbalances (QCMs). The evolution of the etching rates of amorphous carbon (a-C) thin films deposited on the QCMs to mimic contamination are studied as function of operating parameters. We present the results of the plasma cleaning process applied to the real case of a hydrocarbons-contaminated large vacuum vessel. The studies are complemented by transport simulations and surface contamination monitoring by X-ray photoelectron spectroscopy (XPS) analysis. The evaluation of the vessel cleanliness, which is performed via residual gas analysis (RGA) measurements, is based on CERN's outgassing acceptance criteria and agrees with both simulations and XPS results.

## INTRODUCTION

Plasma cleaning is widely employed in the semiconductor industry, the bio-medical sector, and for sample preparation in electron microscopes [1]. This technique has also been used to remove hydrocarbons from accelerator components, particularly in SRF cavities, by generating a glow discharge using oxygen-based gas mixtures [2, 3]. However, the latter approach requires a customized electrodes configuration for each chamber geometry and results of ions with kinetic energy of a few hundred electron volts, clearly above the threshold for physical sputtering. A less invasive alternative consists in exploiting the plasma generated by an RF remote plasma source and injected in the chamber to be treated. In addition, the ion energy remains of the order of a few tens of electron volt, minimizing physical sputtering. However, the cleaning efficiency declines with the distance from the source, due to the loss of active plasma species. Studies evaluating the cleaning rates of carbon-based contaminants as a function of RF powers and distances from the plasma source

have been performed for small chambers or surfaces [4, 5]. In this study we present the cleaning of large accelerator vessels and a first approach in modeling the transport of the active plasma species with COMSOL multiphysics.

## EXPERIMENTAL METHODS

### Plasma Cleaning

We employed inductively coupled plasma (ICP) RF sources branded ibss Group, operating at 13.56 MHz and an RF excitation power  $P_{RF}$  ranging from 10 to 300 W. The gas, pure  $O_2$  (99.999 %), is injected in the ignition chamber of the plasma source and the active species are extracted through an orifice to the volume to be cleaned. The system is kept at constant pressure by turbo pumps. Firstly, the cleaning efficiency was tested in stainless steel chambers with internal diameter (ID) of 100 mm (lengths ranging from 0.1 to 3.5 m), and 600 mm (3.5 m in length) (Fig.1a and Fig.1b). Results are reported for a gas flux of 7 mln/min and a pressure of  $4 \times 10^{-3}$  mbar. The pressure was chosen to be high enough to guarantee stable operation of the plasma source, and sufficiently low to minimize the plasma species deactivation via collisions with the background gas. The optimized treatment was then extended to a stainless steel PSB KFA10 tank presenting a real hydrocarbon contamination, which dimensions are about 2.2 m  $\times$  0.8 m  $\times$  0.44 m. The tank is divided asymmetrically in two chambers that are connected via two 120 mm-diameter apertures. External feed-throughs with an ID of 145 mm were employed to mount the plasma source, the pumping system and an RGA equipped with differential pumping. The treatment was divided into two steps, one mounting the plasma source on the large cell, one on the small cell. Both steps were executed at 300 W, for 5 hours, at a constant  $O_2$  pressure of  $p = 4.3 \times 10^{-3}$  mbar.

### Etching Rate Measurements

The plasma cleaning efficiency was assessed by measuring the etching rates of a-C coatings deposited by magnetron sputtering on top of different QCMs. The QCMs allows to calculate a mass variation per unit area by measuring the change in frequency of a quartz crystal resonator. For each RF power, the etching rate was measured at different distances from the plasma source. The signal of an uncoated QCM was subtracted to correct for thermal drift, the resulting frequency change (Hz/s) was converted into a-C etching rates (nm/s) considering the a-C density ( $1.8 \text{ g/cm}^3$ ) and the QCM active surface. For the ID 100 mm, the length of the chamber was incremented by inserting extra tubular pieces between the two QCMs and the plasma source. In

\* maria.carmen.giordano@cern.ch

the 600 mm-ID tank, lateral feed-throughs at 0.58, 1.89 and 3.2 m from the plasma source were exploited to displace the only a-C coated QCM.

### XPS Measurements

Stainless steel samples of size 1.5 cm × 2 cm were coated with 7 nm of a-C by magnetron sputtering and positioned in the four feed-throughs of the PSB KFA10 (rectangular) tank as witness through the plasma activity during the two steps of the plasma cleaning treatment. A sample named s0 was left untreated as reference. The surface chemical composition of the samples was characterized by XPS in an ESCA5400 system from Physical Electronics using MgK  $\alpha$  radiation ( $h\nu = 1253.6$  eV). The analyzed area was  $\approx 1$  mm in diameter.

### COMSOL Simulations

The plasma cleaning process was treated as a mass transport problem into the chamber to be cleaned. For this scope, we used the COMSOL modules *Heavy Species Transport* of the *Plasma* interface. The mass balance is determined by solving a modified form of the Maxwell-Stefan equation. The mixture averaged diffusion coefficients enter the mass balance equation together with gas convection and reaction kinetics terms, to take into consideration species deactivation mechanisms for the mass conservation. The 20 mm-ID steel aperture and the 40 mm-ID connector to the chamber, present at the outlet of the plasma source, were included in the 3D-modeled chamber geometry as plasma species inlet. The plasma composition at the inlet was set as 75% atomic O, 15%  $O_2(a^1\Delta_g)$ , 10%  $O(^1D)$ , with a overall dissociation rate of 40%, 60% and 80%, for  $P_{RF} = 50, 100$  and 300 W, respectively. These values were defined according to the simulations results of the plasma source itself, set following a model close to ref. [6], here not reported. The concentration of charged species (electrons and ions) was assumed to be negligible outside the plasma source. The reaction mechanisms for the plasma species deactivation are governed by forward rate constants  $k_f$  in the volume and by sticking coefficients  $\gamma_f$  at the walls. Reaction mechanisms and expressions for  $k_f$  were taken from literature for a simplified oxygen chemistry [7]. Values of  $\gamma_f$  were set as 0.1 for O and  $O(^1D)$ , 0.007 for  $O_2(a^1\Delta_g)$  according to the ranges of refs. [7–9]. The simulations were performed at room temperature and a pressure of  $4 \times 10^{-3}$  mbar. The outcome is the spatial distribution of the number density  $n$  of each species involved in the mass balance. The resulting  $n$  for the three active species considered were summed up, the results were extrapolated along specific axis (i.e. the chamber's length) and normalized to the inlet value at  $P_{RF} = 300$  W. The curves here reported start from the inlet position (−6 cm away from the chamber origin).

## RESULTS AND DISCUSSION

In Figure 1, the results of the plasma cleaning efficiency are reported. The simulation results for the 100 mm-ID tubu-

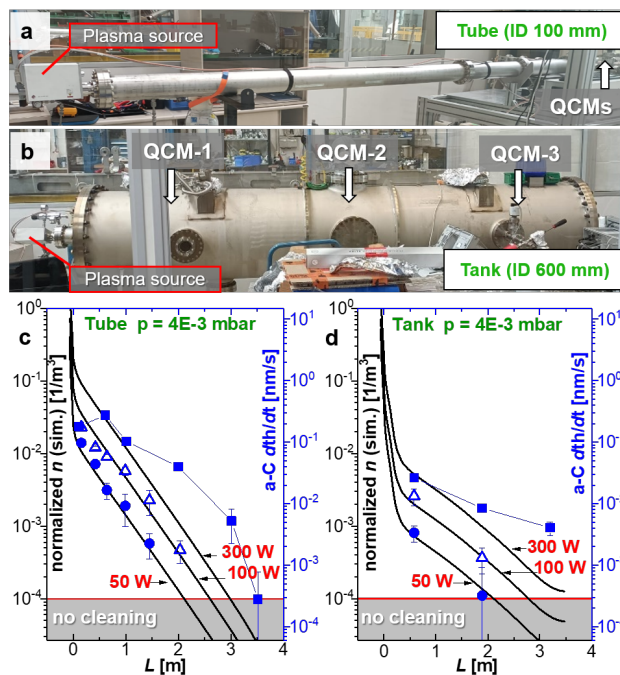


Figure 1: Setup to assess a-C etching rate  $dth/dt$  in (a) 100 mm-ID tubes and (b) a 600 mm-ID tank. Blue symbols are  $dth/dt$  as a function of the distance from the plasma source  $L$  at 50 W (circles), 100 W (triangles), and 300 W (squares) for (c) the 100 mm-ID tubes and (d) the 600 mm-ID tank, compared to the simulation results for plasma species number density  $n$  (black lines).

lar chamber (Fig. 1 c) suggest that the first order of magnitude of plasma species concentration is already lost in the connector between the plasma source outlet and the chamber, while from the position zero where the chamber starts, the species concentration  $n$  decays exponentially with the distance  $L$ . The experimental data of a-C  $dth/dt$  for this geometry show a  $L$ -dependency in agreement with the simulations for  $P_{RF} = 50$  and 100 W. At  $P_{RF} = 300$  W, the measured values deviate considerably, especially for  $L \geq 1.5$  m, and a maximum  $dth/dt$  is recorded at 0.6 m, rather than in proximity of the plasma source. For the 600 mm-ID tank (Fig. 1 d), the simulations predict that, after the connector, a further order of magnitude in the plasma species  $n$  is lost in the first 0.3 m of the chamber. From this position on,  $n$  decreases with an exponential decay and a smaller rate if compared to the curves in the tube. The experimental data agree particularly well at 50 and 100 W and, again, deviate from the simulations at 300 W, for  $L \geq 1.5$  m. The a-C  $dth/dt$  measured values range from  $3 \times 10^{-1}$  nm/s to  $3 \times 10^{-4}$  nm/s, in the 100 mm-ID tube, from  $5 \times 10^{-2}$  nm/s to  $3 \times 10^{-4}$  nm/s, in the 600 mm-ID tank. The latter is the minimum value measured in both chambers. Accordingly, we defined on the simulations y-axis  $1 \times 10^{-4}$  as the limit below which the plasma cleaning is not guaranteed. Both experimental and simulations results suggest that, although a larger volume and wall area in the tank are responsible for the deactivation of a greater number

of plasma species at the chamber entrance, the deactivation then proceeds at a slower rate and species reach slightly greater distances than in the 100 mm-ID tube. While in the volume the deactivation rate mechanisms depends on both the active species concentration and the molecular oxygen one, having opposite trends, the deactivation rate at the walls scales solely with the concentration of active species reaching them. We therefore hypothesize that the wall collisions deactivation is the predominant mechanism by which we lose active species, in the studied pressure regime. The discrepancy we observe at 300 W is still under investigation and may result from having neglected charged species and plasma re-activation mechanisms in the simulations. In Fig-

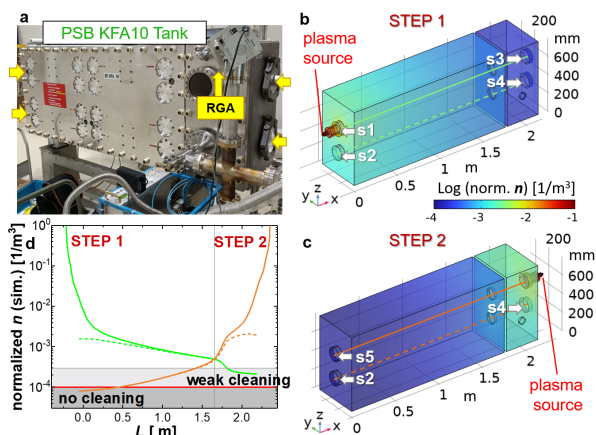


Figure 2: (a) PSB KFA10 tank. Configuration and simulation outcomes for (b) the step 1 and (c) the step 2 of the plasma cleaning procedure. (d) Plasma species  $n$  as function of the distance from the plasma source  $L$  in the two scenarios.

ure 2, we report the simulation results of the plasma cleaning model applied to the peculiar geometry of the PSB KFA10 tank. In Fig. 2a, a picture of the tank is reported, where the position for the four feed-throughs and the RGA are highlighted. Fig. 2b and Fig. 2c represent the configurations for the first and second step of the plasma cleaning treatment, and show the corresponding position for the samples that were analyzed by XPS. The color scale refers to the plasma species  $n$  in case the plasma source is mounted either on the large cell (Fig. 2 b) or the small cell (Fig. 2 c). The depicted solid and dashed lines are the axis for which we extract the  $n$  data, plotted in Fig. 2d. Here, the plasma species distribution along the tank's length  $L$  is reported for both configurations (and steps) of the treatment. According to the simulations results, the combination of the two steps, involving samples s2 and s4, results into a sufficiently high  $n$  to ensure the hydrocarbon (a-C coating) removal from the tank (witness samples). For the most remote point from the plasma source, which is represented by sample s3 for step 1 and by sample s5 for step 2, the simulation foresees, respectively, a weak cleaning and no cleaning of the contamination, in case the single step of the treatment is performed. Table 1 summarizes the plasma cleaning efficiency expected from

the simulations and the surface composition measured by XPS. The carbon signal reduction and synchronous appearance of substrate-related features are reference values for the quantity of remaining surface impurities with 40% of C being the maximum accepted surface content for UHV applications [10]. Consequently, agreement is found between simulations and experiments concerning plasma cleaning performance. Finally, Figure 3 shows the RGA inspection of the tank in the various steps of the procedure and with respect to the limits imposed by CERN's acceptance criteria for non-baked systems (red line) [11]. While the high-masses hydrocarbon peaks show an intensity above the limits before the plasma cleaning treatment, they are well within the limits after the two-steps cleaning procedure.

Table 1: XPS Analysis

Sample	Treatment	Simulations Result	at.% C / substrate <sup>1</sup>
s0	none	-	92.5 / 0
s1	step 1	cleaned	22.4 / 74.4
s2	steps 1 + 2	cleaned	25.9 / 73.9
s3	step 1	weakly cleaned	58.1 / 41.6
s4	steps 1 + 2	cleaned	18.6 / 81.1
s5	step 2	not cleaned	80.9 <sup>2</sup> / 0

<sup>1</sup> The substrate elements are Fe, Cr, O. <sup>2</sup> The reduction of the C content is due to the partial oxidation of the a-C film surface induced by the active species in the plasma.

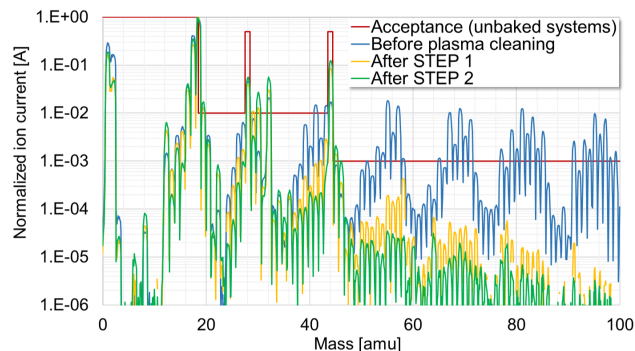


Figure 3: RGA spectra at different stages of the plasma cleaning procedure.

## CONCLUSION

Plasma cleaning is an effective technique for degreasing contaminated surfaces. In this work we successfully demonstrated its applicability for the treatment of 3.5m-long steel tubes and large kicker's tanks, present in different sectors of the CERN's accelerator complex. Cleaning evidences are based on a-C removal rates, XPS-detected surface C content and hydrocarbon peaks decrement in RGA analysis. Our simulations outcomes corroborate qualitatively the experimental results, allowing to predict the success of the plasma cleaning treatment before considering heavier measures such as bake-outs or chemical baths.

## REFERENCES

- [1] D.P.R.Thanu and E. Sekhar Srinadhu and M. Zhao and N. V. Dole and M. Keswani, “Chapter 8 - Fundamentals and Applications of Plasma Cleaning”, in *Developments in Surface Contamination and Cleaning: Applications of Cleaning Techniques*, Rajiv Kohli and K.L. Mittal, Elsevier, 2019, pp. 289–353, [10.1016/B978-0-12-815577-6.00008-6](https://doi.org/10.1016/B978-0-12-815577-6.00008-6).
- [2] A. D Wu *et al.*, “In-situ plasma cleaning to decrease the field emission effect of half-wave superconducting radio-frequency cavities”. *Nuclear Instruments and Methods in Physics Research Section A*, vol. 905, pp. 61-70, 2018, doi: [10.1016/j.nima.2018.07.039](https://doi.org/10.1016/j.nima.2018.07.039)
- [3] S. C. Huang, Q. W. Chu, Y. He, C. L. Li, A. D. Wu, and S. X. Zhang, “The Effect of Helium Processing and Plasma Cleaning for Low Beta HWR Cavity”, in *Proc. SRF'19*, Dresden, Germany, Jun.-Jul. 2019, pp. 1228–1230. doi:[10.18429/JACoW-SRF2019-FRCAB6](https://doi.org/10.18429/JACoW-SRF2019-FRCAB6)
- [4] E. Pellegrin *et al.*, “Characterization, optimization and surface physics aspects of in situ plasma mirror cleaning”. *Journal of synchrotron radiation* vol. 21, Pt 2, pp. 300–14, 2014, doi: [10.1107/S1600577513032402](https://doi.org/10.1107/S1600577513032402).
- [5] H. Moreno Fernández *et al.* “Characterization of carbon-contaminated B4C-coated optics after chemically selective cleaning with low-pressure RF Plasma”. *Scientific Reports* vol. 8, 1293, 2018. doi: [10.1038/s41598-018-19273-6](https://doi.org/10.1038/s41598-018-19273-6)
- [6] <https://www.comsol.com/model/thermal-plasma-8658>
- [7] J. T. Gudmundsson and E. G. Thorsteinsson “Oxygen discharges diluted with argon: dissociation processes. *Plasma Sources Sci. Technol.*, vol. 16, pp. 399–411, 2007, doi:[10.1088/0963-0252/16/2/025](https://doi.org/10.1088/0963-0252/16/2/025)
- [8] M. Mozetič and A. Zalar, “Recombination of neutral oxygen atoms on stainless steel surface”. *Applied Surface Science*, vol. 158, Issues 3–4, pp.263–267, 2000,doi:[10.1016/S0169-4332\(00\)00007-6](https://doi.org/10.1016/S0169-4332(00)00007-6).
- [9] L. Sharpless and T. G. Slange, “Surface chemistry of metastable oxygen. II. destruction of O2 (a1Δg)”. *J. Chem. Phys.*, vol. 91, pp. 7947—7950, 1989, doi:[10.1063/1.457211](https://doi.org/10.1063/1.457211)
- [10] "Procédure de qualification des installations et des procédés de nettoyage UHV". CERN, Geneva, Switzerland. Report 2016-1726970, <https://edms.cern.ch/document/1726970/1>
- [11] G. Cattenoz *et al.*, “Vacuum Acceptance Tests for the UHV Room Temperature Vacuum System of the LHC during LS1”, in *Proc. IPAC'14*, Dresden, Germany, Jun. 2014, pp. 2357–2359. doi:[10.18429/JACoW-IPAC2014-WEPME041](https://doi.org/10.18429/JACoW-IPAC2014-WEPME041)